Research Article
Vol. 28, No. 4 / 17 February 2020 / *Optics Express* 4962
Optics EXPRESS

Detuning effects in Brillouin ring microresonator laser

D. A. KOROBKO,[1,2,*] **I. O. ZOLOTOVSKII,**[1,2] **V. V. SVETUKHIN,**[1,2] **A. V. ZHUKOV,**[1,2] **A. N. FOMIN,**[1,2] **C. V. BORISOVA,**[1,2] **AND A. A. FOTIADI**[1,2,3,4]

[1] *Ulyanovsk State University, 42 Leo Tolstoy Street, Ulyanovsk, 432970, Russian Federation*
[2] *Scientific-Manufacturing Complex "Technological Centre", 1-7 Shokin Square, Zelenograd, Moscow, 124498, Russian Federation*
[3] *Ioffe Physical-Technical Institute, St. Petersburg, 194021, Russian Federation*
[4] *University of Mons, blvd. Dolez 31, Mons, B-7000, Belgium*
[*] *korobkotam@rambler.ru*

Abstract: Brillouin lasers, with their unique properties, offer an intriguing solution for many applications, yet bringing their performance to integrated platforms has remained questionable. We present a theoretical framework to describe Brillouin lasing in integrated ring microcavities. Specifically, a general case of a mismatch between the Brillouin shift and the microresonator inter-mode spacing is considered. We show that although the lasing threshold is increased with the frequency detuning, a significant enhancement of the laser power in comparison with the pure resonant interaction could be achieved. Moreover, there is an optimal pump frequency detuning from the resonant mode frequency, when the effect is most pronounced. An increase of the Brillouin threshold with the pump frequency detuning is accompanied by narrowing the pump frequency range available for lasing. Importantly, at the optimal value of the pump frequency detuning when the Brillouin signal is maximal, Brillouin signal noise level is minimal. Analytical results obtained in the steady-state approach are in quantitative agreement with the results of numerical simulations.

1. Introduction

Spectrally pure lasers are the heart of precision high-end scientific and commercial applications [1–3]. The scope of such laser applications is spread on distributed fiber monitoring [4,5], precise spectroscopy [6], optical communications [7,8], microwave photonics [9], and so on. The most accessible and studied method to narrow the laser linewidth is to organize a feedback loop to the laser generation [10,11], namely a feedback through an external high-Q microresonator [12–14]. The use of such configurations allows to narrow the linewidth of standard semiconductor DFB lasers down to several kHz [15]. Despite the numerous applications, injection-locked lasers currently suffer from rather large linewidth. Brillouin lasers enabling sub-kHz generation linewidth offer an alternative solution. They exploit specific properties of the Brillouin scattering amplification process such as a low-power threshold and a narrow gain band (tens of MHz) [16]. Such a narrow Brillouin gain spectrum that could be narrower than the microresonator inter-mode spacing supports single-frequency Brillouin laser operation in fiber cavities of lengths less than ~10 m [17,18]. Currently, Brillouin lasers are poised to make the leap from the fiber structures to integrated circuits [19]. Translating their performance to integrated photonics will dramatically reduce cost and footprint for applications such as ultrahigh capacity fiber and data center networks, atomic clocks and sensing [20]. Recently, a sub-hertz (~0.7 Hz) fundamental linewidth Brillouin laser in an integrated Si_3N_4 waveguide platform has been demonstrated that translates advantages of non-integrated designs to the chip scale [21]. Such silicon-foundry-compatible design supports low loss from 405 to 2350 nm and can be integrated with other components, in particular, based

#382357
Journal © 2020
https://doi.org/10.1364/OE.382357
Received 4 Nov 2019; revised 20 Dec 2019; accepted 21 Dec 2019; published 7 Feb 2020

on silicon, chalcogenide glasses, and other materials with high Brillouin gain factor [22–24]. Single- and multiple-frequency output operation provides a versatile low phase-noise solution. Effective Brillouin lasing in microcavities requires adjusting the microresonator inter-mode frequency spacing (i.e. a multiple free spectrum range (FSR)) to the Brillouin frequency shift. Both these parameters depend on the pump wavelength and external factors (temperature, strain, etc.). The current advanced technology allows tuning the FSR with an accuracy of about 1 MHz (through a control of the microresonator size), while its absolute value is comparable with the Brillouin frequency shift (typically, ~10 GHz) [24]. The effects of the inter-mode frequency spacing detuning from the Brillouin shift on Brillouin lasing should be mandatorily taken into account by the laser designers. In particular, a chip integrable silica microdisk Brillouin laser has been recently demonstrated as a part of a dual-microcavity system enabling laser generation of a superior spectral purity [25]. In that system one silica microresonator is used for lasing, while the second microcavity helps suppress the phase noise and stabilize the laser frequency through operation of the feedback loop. The frequency detuning effects are vital for the stabilization algorithms used in such systems. They should be also important for organizing the laser frequency scanning, adjustment of the Brillouin frequency combs [26] and sensing external quantities [27].

The aim of this work is to describe the dynamical effects arising in the Brillouin laser microcavities in the case of offset between the Brillouin frequency shift and the microresonator FSR ranging $\pm FSR/2$ to exclude mode-hopping events. Formally, the used approach is valid for description of backward single-frequency Brillouin lasers with a micro-resonator shorter than one meter. However, the target objects of our treatment are cavities of smaller size, like microcavities based on an integrated waveguide platform, that are subjected to an extended frequency detuning in GHz range still remaining in the frame of our consideration. Although our detailed calculations have been performed for a silica disk employing parameters of the real experimental geometry [25], in general, the used approach is applicable for a wide range of the integrated devices operating Brillouin interactions as the strongest nonlinearity. For example, the silicon-based resonators should be considered with caution since Brillouin interactions are markedly weak in conventional silicon photonic waveguides due to nonlinear losses in silicon [28,29,30] that are not taken into account by the model. However, the recent advent of hybrid silicon photonic-phononic waveguides [31] with dominating Brillouin interactions makes the model applicable for such structures as well. Remarkable progress in silicon-based Brillouin waveguides has been made recently through the integration of a high Brillouin gain material, As_2S_3, onto a silicon-based chip [32]. A ring Brillouin laser fabricated with free spectral range matched to the Brillouin shift with a compact spiral device within a silicon circuit is a potential object of the detuning effects as soon as the parameters of the real experimental geometry [33] are applied. Formally, the used approach is not applicable for forward Brillouin scattering [31,34]. Besides, cascade generation of the multi-order Brillouin components [35] ignored in our consideration is assumed to be technically excluded (using additional filters, for example).

2. Coupled Brillouin equations

The configuration of the Brillouin laser is shown in Fig. 1(a). The microresonator is pumped from a strongly monochromatic laser source at the frequency ω_P exciting a pump optical wave for clockwise propagation inside the microresonator. The counterclockwise Stokes wave is generated through the Brillouin process at the frequency and propagates inside the microresonator in counter clock wise direction. Following [36] the Brillouin process could be described in 1-D approach as an interaction between the complex amplitudes $A_F(t)$ and $A_B(t)$ of two optical microresonator modes at frequencies ω_F and , respectively, through a hypersound wave $\rho(t)$ at the frequency Ω (see, Fig1(a, b)):

$$\begin{aligned}
\frac{\partial A_F}{\partial t} &= -\frac{A_F}{2\tau_F} - i\frac{\gamma_e \omega_F}{4n_0^2\rho_0} K A_B \rho + \sqrt{\frac{P}{\tau_{ext}}} \exp(i(\omega_P - \omega_F)t) \\
\frac{\partial A_B}{\partial t} &= -\frac{A_B}{2\tau_B} - i\frac{\gamma_e \omega_B}{4n_0^2\rho_0} K A_F \rho^* \\
\frac{\partial \rho}{\partial t} &= i\frac{\Omega_b^2 - \Omega^2}{2\Omega}\rho - \frac{\Gamma}{2}\rho - i\frac{\varepsilon_0 \gamma_e}{4\Omega}\frac{\ell_\rho^2}{R^2} K A_F A_B^*
\end{aligned} \tag{1}$$

where ω_F is considered to be the nearest to ω_P microresonator mode frequency; K is the overlapping integral describing efficiency of the mode coupling; Ω_b is the central Brillouin frequency shift; γ_e is the electrostriction coefficient; n_0 is the waveguide refractive index. In the transverse cross-section the optical modes are assumed to be the fundamental waveguide modes. The radius of the mode trajectory is assumed to be the radius of the microresonator R; ℓ_F, ℓ_B and ℓ_ρ are angular moments for the clockwise, Stokes and hypersound waves, respectively. Since Eq. (1) describes interaction of the optical modes, the angular moments ℓ_F and ℓ_B satisfy to $l_F = 2\pi R/m_F$ and $l_B = 2\pi R/m_B$, where m_F and m_B are fixed integers. The phase matching conditions are satisfied assigning $\Omega = \omega_F - \omega_B$ and $\ell_\rho = \ell_F + \ell_B$. For simplicity we set $K = 1/2$ [36]. The time constants τ_F and τ_B are lifetimes for the clockwise and counterclockwise optical waves describing losses in the microresonator. These losses are superposition of the losses caused by coupling with the input-output waveguide and the material losses. So, for the clockwise and counterclockwise waves the lifetime constants are:

$$\frac{1}{\tau_F} = \frac{1}{\tau_{ext}} + \frac{1}{\tau_{F,0}},$$

$$\frac{1}{\tau_B} = \frac{1}{\tau_{ext}} + \frac{1}{\tau_{B,0}}.$$

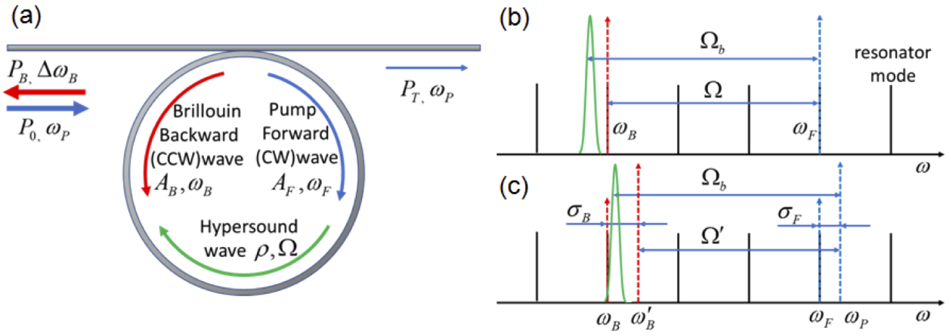

Fig. 1. Scheme of the Brillouin lasing in a microresonator (a). The optical resonances in the ring cavity illustrating Brillouin interaction and frequency detuning of pump (blue) and Brillouin (red) waves described by Eq. 1 (b) and Eq. 3 (c). Green curve illustrates the gain spectrum.

The energies of the clockwise and counterclockwise waves in the microresonator, $|A_F|^2$ and $|A_B|^2$, respectively, are linked as [37]:

$$\frac{|A_B|^2}{\tau_B} + \frac{|A_F|^2}{\tau_{0,F}} = P - P_T, \tag{2}$$

where, P is the pump power and P_T is the optical power reflected by the microresonator.

Considering the pump (and so, clockwise) wave frequency detuning from the optical resonance $\sigma_F = \omega_P - \omega_F$, we also allow offsets to counterclockwise wave and hypersound wave frequencies

$\sigma_B = \omega'_B - \omega_B$, $\sigma_\rho = \Omega' - \Omega$, respectively. New phase-matching is achievable at $\sigma_F = \sigma_B + \sigma_\rho$ (see, Fig. 1(c)). With new slowly varying complex amplitudes $A'_F = A_F \exp(-i(\sigma_F t + \varphi_F))$, $A'_B = A_B \exp(-i(\sigma_B t + \varphi_B))$ and $\rho' = \rho \exp(-i(\sigma_\rho t + \varphi_\rho))$, where φ_i are functions of t ($i \equiv F, B, \rho$), the Eq. (1) could be replaced by:

$$\begin{aligned}
\frac{\partial|A_F|}{\partial t} &= -\frac{|A_F|}{2\tau_F} + \frac{\gamma_e\omega_0}{8n_0^2\rho_0}|A_B||\rho|\sin(\varphi_\rho + \varphi_B - \varphi_F) + \sqrt{\frac{P}{\tau_{ext}}}\cos(\varphi_P - \varphi_F)\\
\frac{\partial\varphi_F}{\partial t} &= -\sigma_F - \frac{\gamma_e\omega_0}{8n_0^2\rho_0}\frac{|A_B||\rho|}{|A_F|}\cos(\varphi_\rho + \varphi_B - \varphi_F) + \sqrt{\frac{P}{\tau_{ext}}}\frac{\sin(\varphi_P - \varphi_F)}{|A_F|}\\
\frac{\partial|A_B|}{\partial t} &= -\frac{|A_B|}{2\tau_B} + \frac{\gamma_e\omega_0}{8n_0^2\rho_0}|A_F||\rho|\sin(\varphi_F - \varphi_B - \varphi_\rho)\\
\frac{\partial\varphi_B}{\partial t} &= -\sigma_B - \frac{\gamma_e\omega_0}{8n_0^2\rho_0}\frac{|A_F||\rho|}{|A_B|}\cos(\varphi_F - \varphi_B - \varphi_\rho)\\
\frac{\partial|\rho|}{\partial t} &= -\frac{\Gamma}{2}|\rho| + \frac{\varepsilon_0\gamma_e}{8\Omega}\frac{\ell_\rho^2}{R^2}|A_F||A_B|\sin(\varphi_F - \varphi_B - \varphi_\rho)\\
\frac{\partial\varphi_\rho}{\partial t} &= -\sigma_\rho + \frac{\Omega_b^2 - \Omega^2}{2\Omega} - \frac{\varepsilon_0\gamma_e}{8\Omega}\frac{\ell_\rho^2}{R^2}\frac{|A_F||A_B|}{|\rho|}\cos(\varphi_F - \varphi_B - \varphi_\rho).
\end{aligned} \tag{3}$$

where, $\omega_B \approx \omega_F = \omega_0$.

3. Steady-state solution

Unlike Eq. (1), the steady-state solution for Eq. (3) could be found as

$$\begin{aligned}
|A_F|^2 &= \frac{16n_0^2\rho_0\Gamma\Omega R^2}{\tau_B\varepsilon_0\gamma_e^2\omega_0\ell_\rho^2}\frac{1}{\sin^2(\varphi_F - \varphi_B - \varphi_\rho)},\\
|A_B|^2 &= \frac{2\tau_B}{\sqrt{\tau_{ext}}}\sqrt{P}|A_F|\cos(\varphi_P - \varphi_F) - \frac{\tau_B}{\tau_F}|A_F|^2.
\end{aligned} \tag{4}$$

One can see that in steady-state, the energy of the clockwise wave does not depend on the pump power. It is just determined by the phase mismatch of the interacting waves and by the microresonator parameters. The equation for $|A_B|^2$ in Eq. (4) constitutes the energy conservation, since $A_F / \sqrt{\tau_{ext}} = \sqrt{P} + \sqrt{P_T}$ (see, Eq. (2)) [37]. The pump and Brillouin wave powers are connected through Eq. (2) as:

$$\frac{|A_B|^2}{\tau_{ext}} = \frac{\tau_B}{\tau_{ext}}\left(P - P_T - \frac{|A_F|^2}{\tau_{0,F}}\right). \tag{5}$$

Therefore, the parameters τ_B / τ_{ext} and $|A'_F|^2 \Big/ \tau_{0,F}$ regulate the efficiency of lasing and threshold power, respectively.

In a general (non-resonant) case ($\Omega_b > \Omega$), the dependences of the optical energies on the frequency offset σ_F could be found from the phase matching conditions and Eq. (3):

$$\begin{aligned}
\sigma_B &= \frac{\sigma_F - ((\Omega_b^2 - \Omega^2)/2\Omega)}{1 + \Gamma\tau_B},\\
\sigma_\rho &= \frac{\sigma_F\Gamma\tau_B + ((\Omega_b^2 - \Omega^2)/2\Omega)}{1 + \Gamma\tau_B}.
\end{aligned} \tag{6}$$

The Brillouin laser frequency is determined by the difference between the Brillouin shift and the inter-mode spacing $\Omega_b - \Omega$ and by the detuning σ_F. The frequency offsets disturb phase relations between the interacting waves changing the system steady-state. Indeed, when $\Omega_b = \Omega$, zero pump wave detuning means that $\sigma_B = \sigma_\rho = 0$ and so, in steady-state, $\varphi_F - \varphi_B - \varphi_\rho = \pi/2$ and $\varphi_P - \varphi_F = 0$. Any frequency detuning changes the phase relations followed by a change of system steady-state, in particular, the waves energies.

The implicit and explicit expressions for the clockwise and counterclockwise wave energies as functions of the frequency offset could be obtained from Eq. (3):

$$\sin^2(\varphi_F - \varphi_B - \varphi_\rho) = \frac{1}{1 + 4\tau_B^2\sigma_B^2},$$

leading to:

$$\begin{aligned}
&|A_F|^2 = \tfrac{g}{\tau_B}\left(1 + \left(\tfrac{2(\sigma_F-\Delta)\tau_B}{1+\Gamma\tau_B}\right)^2\right),\\
&|A_B|^2 = \sqrt{\tfrac{4g\tau_B P}{\tau_{ext}}(1+(2\sigma_B\tau_B)^2)}\,\cos(\varphi_P-\varphi_F) - \tfrac{\tau_B}{\tau_F}|A_F|^2,\\
&\cos(\varphi_P - \varphi_F) = \left|\tfrac{\sqrt{1+(2\sigma_B\tau_B)^2}}{2\tau_F} + \tfrac{\frac{|A_B|^2}{2g}}{\sqrt{1+(2\sigma_B\tau_B)^2}}\right| \times\\
&\times\left((1+(2\sigma_B\tau_B)^2)\left(\sigma_F^2 + \left(\tfrac{1}{2\tau_F}\right)^2\right) + \tfrac{|A_B|^2}{2g}\left(\tfrac{1}{\tau_F} - 4\sigma_F\sigma_B\tau_B\right) + \tfrac{|A_B|^4}{4g^2}\right)^{-1/2},
\end{aligned} \tag{7}$$

where, $\Delta = (\Omega_b^2 - \Omega^2)/2\Omega$ and $g = 16\rho_0\Gamma\Omega n_0^2 R^2 / \omega_0\varepsilon_0\gamma_e^2\ell^2$.

Although this formalism is applicable for a wide range of the integrated devices, below we use it to analyze behavior of the Brillouin lasing at $\lambda = 1550$ nm ($\omega_0 = 1.22 \cdot 10^{15}$) in a chip integrable pure silica microdisk. Such laser design has been recently reported [25] as a part of the dual-microcavity laser system delivering radiation of a superior spectral purity. With the microresonator radius of ~2.8 mm and mode area of 25 μm^2 [36] the pump power of 1 mW and 3 mW corresponds to $P = 2.3 \cdot 10^{20}\mathrm{W}/(\mathrm{m}^2\mathrm{F})$ and $P = 6.9 \cdot 10^{20}\mathrm{W}/(\mathrm{m}^2\mathrm{F})$, respectively. Table 1 lists other system parameters.

Table 1. Parameters of the microresonator

Parameter	Value	Parameter	Value
$\tau_F = \tau_B$	$(2\pi \cdot 2 \cdot 10^6)^{-1}s$	γ_e	1.5
τ_{ext}	$(2\pi \cdot 1.33 \cdot 10^6)^{-1}s$	n_0	1.5
Γ	$(2\pi \cdot 15.64 \cdot 10^6)s^{-1}$	ρ_0	2200 kg/m^3
Ω_b	$(2\pi \cdot 11.55 \cdot 10^9)s^{-1}$	ℓ/R	$1.22 \cdot 10^7$ m^{-1}

First, let us consider the resonant case ($\Omega_b = \Omega$), when the Brillouin shift is exactly the spectral spacing between two microresonator modes (i.e. a multiple FSR). Figure 2(a) display the clockwise and counterclockwise waves energies as functions of the pump detuning frequency σ_F. The energy of the clockwise wave increases parabolically with the detuning σ_F. The curve is symmetrical in respect to σ_F sign. In agreement with Eq. (4) the clockwise wave energy does not depend on the pump power. At low pump powers, the threshold value of the clockwise wave energy is minimal at zero detuning σ_F. Generation of the counterclockwise wave occurs in a narrow spectrum range $\sigma_B \to 0$. Importantly, the band of possible changes of σ_B in $1 + \Gamma\tau_B$ narrower than the band bounded between two threshold points of σ_F (see Eq. (6)). An increase of the pump power increases the energy of the counterclockwise wave and broadens the spectrum range available for the counterclockwise wave generation. The spectrum band bounded between two threshold points of σ_F also increases. Note, the dependence of the counterclockwise wave energy on the Brillouin frequency detuning is almost flat. In other words, there is an extended Brillouin frequency range, where the counterclockwise wave energy does not depend on the pumping frequency.

Let us now compare the considered resonant case with the case when the Brillouin shift exceeds the microresonator inter-mode spacing $\Omega_b > \Omega$ (Fig. 2(b)). In this non-resonant case, the frequency of counterclockwise wave is pulled toward to the peak of the gain spectrum [38].

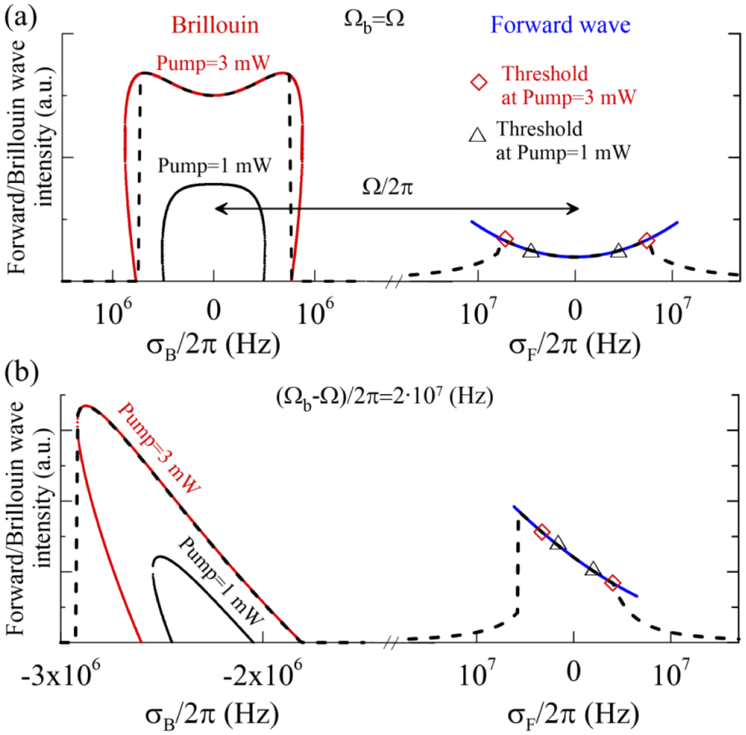

Fig. 2. (a) The steady-state Brillouin wave energy as function of the detuning σ_B for different pump powers (left) and the clockwise wave energy as function of the detuning σ_F (right) for the resonant case ($\Omega_b = \Omega$) when the Brillouin frequency shift is a multiple microcavity FSR. (b) The same, but for non-resonant case when the Brillouin shift is detuned by $(\Omega_b - \Omega)\big/ 2\pi = 20$. Symbols denote clockwise wave energy levels corresponding to the Brillouin threshold. The results of numerical simulation (Eq. (3)) (dashed) at the pump power of 3 mW. Note, scales for σ_B (left) and σ_F (right) are different.

For example, the detuning $\Delta/2\pi = 20$ MHz shifts the Brillouin generation band by 2.5–3 MHz. The dependence of the clockwise wave energy on σ_F is not symmetrical anymore, the minimum of the parabola is shifted to the point $\sigma_F = \Delta$. The clockwise wave energy is higher, the band of σ_F available for laser generation is narrower than in the resonant case. Accordingly, the generation band of available σ_B is narrower as well. Moreover, there is a spectrum range where the dependence of energy $|A_B|^2$ on the Stokes frequency detuning σ_B is double-valued. However, the top branch only corresponds to a stable solution. The maximum of the counterclockwise wave energy is localized in the band corresponding to minimal σ_B values limited by the condition of $\cos(\varphi_P - \varphi_F) = 1$. It highlights the frequency pulling effect. Importantly, there is a range Δ, where at sufficiently high pump powers the maximum value of the counterclockwise wave energy exceeds the level obtained for the resonant case $\Delta = \sigma_B = \sigma_F = 0$. In particular, one can see from Fig. 2 that at $\Delta/2\pi = 20$ MHz, the pumping with a power higher than 1 mW causes an increase of the lasing wave peak energy in comparison with the resonant case $\Delta = \sigma_B = \sigma_F = 0$. Assuming that the detuning Δ is high enough for pulling to overtake the characteristic losses $\sigma_B > 1/\tau_B$, we can estimate the parameters enabling the increasing of Brillouin power:

$$\frac{(2\sigma_B\tau_B - 1)}{2(\sigma_B\tau_B)^2} > \frac{1}{\tau_F}\sqrt{\frac{g\tau_{ext}}{P\tau_B}}.$$

4. Numerical modelling

In this section we present results of numerical simulation of Eq. (3) and compare them with the results of steady-state analysis. To simulate generation of the Brillouin wave from the noise level a term describing low thermal density fluctuations (Langevin noise source) has been added to the equation for hypersound wave in Eq. (1). The Langevin white noise source $f(t)$ equally contributes the real f_r and imaginary f_i parts $\left\langle f_r(t) f_r^*(t') \right\rangle = C\delta(t'-t)$, where $C = kT\rho_0\Gamma \big/ V\upsilon^2$, V is the volume of the acoustic mode, k is the Boltzmann constant, υ is the speed of the hypersound [39]. In the steady-state lasing regime the noise term implies the amplitude and phase fluctuations of the interacting waves. Without the noise the interacting waves are completely coherent. Evolution of the interacting wave energies from the zero to the steady-state level have been simulated at different pump power levels employing 4-order Runge-Kutta algorithm.

The simulation results corresponding to the theoretical consideration at the pump power of 3 mW are presented in Fig. 2. In the both resonant ($\Omega_b = \Omega$) and non-resonant ($\Omega_b > \Omega$) cases they well fit the steady-state curves of Eq. (7). The only difference is the parts of the curves corresponding to instable solutions that are omitted in simulations. Besides, the simulation curve is extended to the σ_F ranges, where lasing does not occur, since the clockwise wave energy is below the threshold.

Let us analyze how the Brillouin lasing in microresonator changes with an increase of the pump power. Considering the resonant case ($\Omega_b = \Omega$). The transmission of the microresonator P_T / P as a function of the frequency detuning σ_F shown in Fig. 3(a) is defined by Eq. (2). At low $P \to 0$, it corresponds to the transmission spectrum of the microresonator determined by $\tau_{F,0}$ and τ_{ext} only (dotted line in Fig. 3(a)). As the pump power increases and the counterpropagating wave is generated, the detuning σ_B becomes linked to the detuning σ_F (Eq. (6)). The pump power efficiently transfers to the counterclockwise wave energy. The transmittance of the microresonator increases and gets maximum. Therefore, within whole pump frequency detuning band available for lasing the energy of the clockwise wave does not depend longer on the pump power. The simulation results well reproduce these analytical predictions based on the steady-state approximation. Besides, in terms of optical powers and spectral bands, the results are in agreement with the experimental observations [25].

Figure 3(b) depicts the output power of the generated wave $|A_B|^2 \big/ \tau_{ext}$ as a function of the pump power. One can see that with zero detuning σ_F the pump power threshold is minimal. From Eq. (4) it is expressed as:

$$P_0 = \frac{g\tau_{ext}}{4\tau_B\tau_F^2}.$$

Decreasing of the microresonator transmission P_T / P with the pump power in accordance with Eq. (5), leads to decreasing of the differential generation efficiency. As predicted analytically from the steady-state solution, the lasing threshold increases with non-zero pump frequency detuning. Surprisingly, at non-zero pump frequency detuning there is a pump power level at which the output laser power exceeds its value at $\sigma_F = 0$. It is also in agreement with the prediction of steady-state solution Eq. (7) (see Fig. 2(a)) that the energy level $|A_B|^2$ corresponding to the non-zero detuning values exceeds its value in the central part at $\sigma_F = 0$.

In the non-resonant case ($\Omega_b > \Omega$) the transmission curve shown in Fig. 3(c) possesses asymmetry highlighting the frequency pulling. The clockwise and counterclockwise waves energies are well approximated by the analytical expressions based on Eq. (7). With a fixed pump power level, the detuning σ_F available for lasing is narrower than in the resonant case ($\Omega_b = \Omega$). Narrowing the detuning range of available σ_F causes corresponding narrowing the range of available frequencies σ_B. These effects are explained by the increase of the pump threshold power in comparison with the resonant case ($\Omega_b = \Omega$) that is high enough even for resonant pumping $\sigma_F = 0$. Moreover, the threshold increases with the detuning σ_F. Thus, the

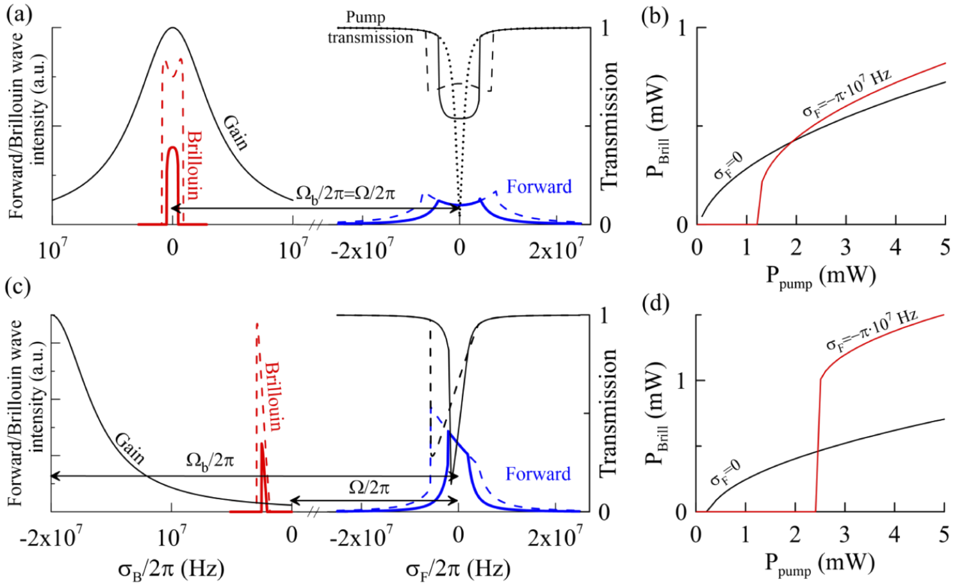

Fig. 3. (a) The fractions of the pump wave power inside the microresonator and reflected by the microresonator as functions of the pump frequency detuning σ_F (right). The Brillouin wave intensity as a function of σ_B (left). Pump power is 1 mW (solid), 3 mW (dashed). The microresonator transmittance without Brillouin lasing (dotted). (b) The Brillouin laser power as a function of the pump power at various offsets σ_F. The spectral distance between the clockwise and counterclockwise waves coincides with the SBS-shift (a, b). The resonant case ($\Omega_b = \Omega$) (a, b) and non-resonant case with $(\Omega_b - \Omega)\big/2\pi = 20$MHz (c, d) are shown.

enhanced threshold allows to achieve much higher lasing power than in the resonant case $\Omega_b = \Omega$ (Fig. 3(d)).

Figure 4 provides more details of the reported effect. It evaluates the clockwise and counterclockwise wave energies as functions of the frequency offsets at different values of $\Omega_b - \Omega$. In agreement with Eq. (6) the dependence of the detuning σ_B on the value $\Omega_b - \Omega$ is linear. A drastic increase of the clockwise wave intensity followed by narrowing the band of σ_F available for lasing and fast rise of the clockwise wave intensity just above the threshold are also in agreement with

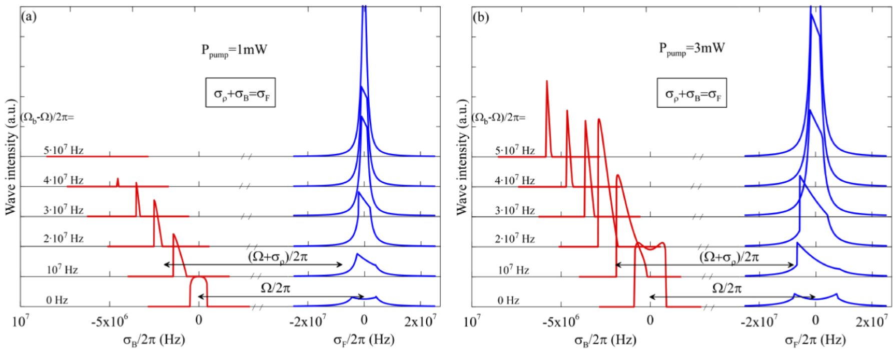

Fig. 4. The intensities of the clockwise and counterclockwise waves as functions of the detuning σ_F and σ_B, respectively, at different values of $(\Omega_b - \Omega)/2\pi$. The pump power is 1 mW (a), 3 mW (b). Note, different scales are used with σ_F and σ_B.

the previous observations. Figure 4 confirms the specific feature established above: in a certain range of detuning $(\Omega_b - \Omega)$ and at a sufficiently high pump power levels, the maximum value of the lasing wave energy is higher in comparison with its value in resonance $\Delta = \sigma_B = \sigma_F = 0$. The pumping power of 1 mW is quite enough to increase the peak energy of the counterclockwise wave in the detuning range of $0 < (\Omega_b - \Omega) / 2\pi \leq 30$ MHz. The absolute maximum energy $|A_B|^2$ is fixed at the pump detuning $\sigma_F \approx 1.5$MHz and $(\Omega_b - \Omega) / 2\pi = 20$ MHz. With a further $(\Omega_b - \Omega)$ increase the lasing energy falls rapidly. With the pump power increased to 3 mW, the maximal value of possible Brillouin wave detuning σ_B available for lasing increases significantly. In the whole considered range $0 < (\Omega_b - \Omega) / 2\pi \leq 50$MHz the maximum of the lasing wave energy exceeds its value at the resonance $\Omega_b = \Omega$. The absolute maximum of the lasing wave energy is achieved at the pump frequency detuning $\sigma_F \approx 3$MHz and $(\Omega_b - \Omega) / 2\pi = 20$MHz.

5. Noise performance of the Brillouin microlaser

We have also performed numerical simulations in order to evaluate the noise properties of the laser radiation emitted by the microresonator. The RIN (relative intensity noise) spectral density of the laser radiation is defined as

$$S(\omega) = \frac{2}{\left\langle |A_B|^2 \right\rangle^2} \int_{-\infty}^{+\infty} \left\langle \delta |A_B(t)|^2 \delta |A_B(t+\tau)|^2 \right\rangle \exp(i\omega\tau) d\tau.$$

This quantity has been evaluated in the cases of $(\Omega_b - \Omega) / 2\pi = 0$ and $(\Omega_b - \Omega) / 2\pi = 20$ MHz, and at different pump frequency detuning σ_F. The simulation has been performed with the pump power of 3 mW. In the resonant case $(\Omega_b = \Omega)$ (Fig. 5(a)) the flat dependence of the laser noise intensity on the frequency detuning extended up to 10 MHz causes a weak dependence of the RIN spectral density on the pump frequency detuning σ_F. The RIN is approximately -137 dB/Hz at $\sigma_F = 0$, and then increases with σ_F. At $\sigma_F / 2\pi = 5$ MHz the RIN is approximately -125 dB/Hz.

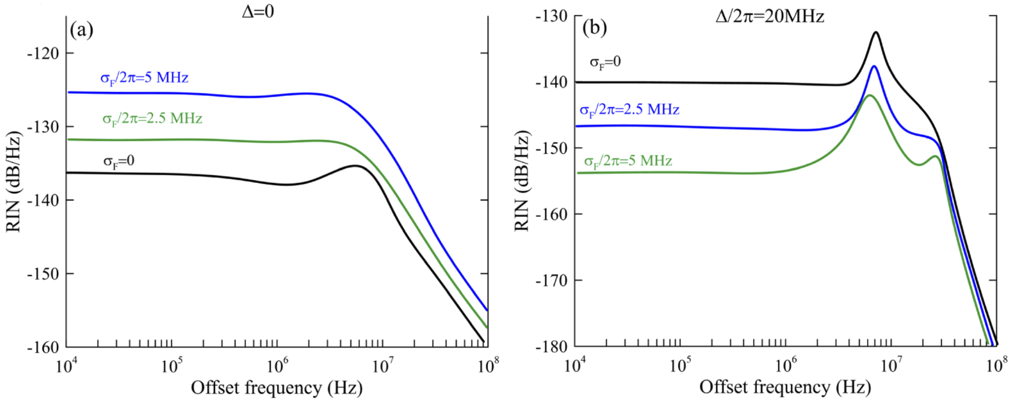

Fig. 5. The relative noise intensity (RIN) spectral density for the Brillouin lasing in microresonator at different pump frequency detuning. The resonant case $(\Omega_b = \Omega)$ (a) and non-resonant case with $(\Omega_b - \Omega) / 2\pi = 20$MHz (b).

Surprisingly, in a non-resonant case, the RIN of the emitted radiation could be significantly reduced as an optimal non-zero pump frequency detuning is used. It can be seen in Fig. 5(b) the pump frequency detuning of $\sigma_F / 2\pi = 5$MHz reduces the RIN level down to -153 dB/Hz, i.e. by ~13 dB/Hz in respect to the resonant pumping $(\sigma_F = 0)$ and by ~16 dB/Hz in respect to the resonant case $(\Omega_b = \Omega)$. This effect is explained by narrowing the laser generation band followed by suppression of the laser power response to the phase and amplitude noise fluctuations at the pump frequency detuning σ_F corresponding the maximal energy conversion to the generated wave. Despite a strong phase-amplitude coupling observed as a pronounced peak near 5-6 MHz (Fig. 5(b)), in a wide frequency band of 10 kHz -50 MHz the RIN level is lower than in the resonant case. So, the optimal pump frequency detuning allows to improve the noise performance of the Brillouin microlaser.

6. Conclusion

We have reported on the analytical treatments and computer simulations of Brillouin lasing in integrated microresonator. In contrast to the previous works [36,40], we focus on a non-resonant case, when the Brillouin frequency shift is not a multiple of the microresonator inter-mode spacing. In particular, we have explored that despite an increase of the lasing threshold power and pulling the gain maximum from the optical mode, the lasing intensity can be higher in the non-resonant case than in the resonant one. To enable the enhanced lasing the pump frequency should be detuned from the resonant mode frequency providing an optimal detuning. Apart increase of the lasing threshold power, narrowing of the detuning frequency range available for lasing also occurs in the non-resonant case. Moreover, when the pump frequency detuning is optimized, the Brillouin laser noise is reduced. Analytical results are in good agreement with the numerical simulations and do not contradict the experimental observations [25]. The results of the work are important for design of Brillouin micro-lasers with improved performance characteristics in integrated circuits where cascaded generation of the high-order Brillouin component is technically excluded. In particular, the interconnection between the pump and Stokes frequencies explored here in the terms of σ_F, σ_B (for the cases of resonant and nonresonant Brillouin interaction) is important for implementation of advanced stabilization algorithms enabling laser generation of a superior spectral purity [25].

Funding

Ministry of Education and Science of the Russian Federation (State task 2019 for SMC “Technological Centre”); Russian Science Foundation (18-12-00457).

Disclosures

The authors declare no conflicts of interest.

References

1. B. Stern, X. Ji, A. Dutt, and M. Lipson, “Compact narrow-linewidth integrated laser based on a low-loss silicon nitride ring resonator,” Opt. Lett. **42**(21), 4541–4544 (2017).
2. R. Legaie, C. J. Picken, and J. D. Pritchard, “Sub-kilohertz excitation lasers for quantum information processing with Rydberg atoms,” J. Opt. Soc. Am. B **35**(4), 892–898 (2018).
3. T. Komljenovic, M. Davenport, J. Hulme, A. Y. Liu, C. T. Santis, A. Spott, and J. E. Bowers, “Heterogeneous silicon photonic integrated circuits,” J. Lightwave Technol. **34**(1), 20–35 (2016).
4. D. Leandro, V. deMiguel-Soto, and M. López-Amo, “High-resolution sensor system using a random distributed feedback fiber laser,” J. Lightwave Technol. **34**(19), 4596–4602 (2016).
5. J. L. Bueno Escobedo, V. V. Spirin, C. A. López-Mercado, A. Márquez Lucero, P. Mégret, I. O. Zolotovskii, and A. A. Fotiadi, “Self-injection locking of the DFB laser through an external ring fiber cavity: Application for phase sensitive OTDR acoustic sensor,” Results Phys. **7**, 641–643 (2017).
6. D. K. Shin, B. M. Henson, R. I. Khakimov, J. A. Ross, C. J. Dedman, S. S. Hodgman, and A. G. Truscott, “Widely tunable, narrow linewidth external-cavity gain chip laser for spectroscopy between 1.0–1.1 µm,” Opt. Express **24**(24), 27403–27414 (2016).
7. Z. Fang, H. Cai, G. Chen, and R. Qu, *Single frequency semiconductor lasers*. Springer Singapore (2017).
8. H. Guan, A. Novack, T. Galfsky, Y. Ma, S. Fathololoumi, A. Horth, and Y. Liu, “Widely-tunable, narrow-linewidth III-V/silicon hybrid external-cavity laser for coherent communication,” Opt. Express **26**(7), 7920–7933 (2018).
9. D. Marpaung, J. Yao, and J. Capmany, “Integrated microwave photonics,” Nat. Photonics **13**(2), 80–90 (2019).

10. J. Mork, B. Tromborg, and J. Mark, "Chaos in semiconductor lasers with optical feedback: theory and experiment," IEEE J. Quantum Electron. **28**(1), 93–108 (1992).
11. K. Petermann, "External optical feedback phenomena in semiconductor lasers," IEEE J. Sel. Top. Quantum Electron. **1**(2), 480–489 (1995).
12. J. Lim, A. A. Savchenkov, E. Dale, W. Liang, D. Eliyahu, V. Ilchenko, and C. W. Wong, "Chasing the thermodynamical noise limit in whispering-gallery-mode resonators for ultrastable laser frequency stabilization," Nat. Commun. **8**(1), 8 (2017).
13. H. Erzgräber, B. Krauskopf, D. Lenstra, A. P. A. Fischer, and G. Vemuri, "Frequency versus relaxation oscillations in a semiconductor laser with coherent filtered optical feedback," Phys. Rev. E **73**(5), 055201 (2006).
14. C. A. López-Mercado, V. V. Spirin, J. L. Bueno Escobedo, A. Márquez Lucero, P. Mégret, I. O. Zolotovskii, and A. A. Fotiadi, "Locking of the DFB laser through fiber optic resonator on different coupling regimes," Opt. Commun. **359**, 195–199 (2016).
15. J. L. Bueno Escobedo, V. V. Spirin, C. A. López-Mercado, P. Mégret, I. O. Zolotovskii, and A. A. Fotiadi, "Self-injection locking of the DFB laser through an external ring fiber cavity: Polarization behavior," Results Phys. **6**, 59–60 (2016).
16. A. Kobyakov, M. Sauer, and D. Chowdhury, "Stimulated Brillouin scattering in optical fibers," Adv. Opt. Photonics **2**(1), 1–59 (2010).
17. E. Garmire, "Perspectives on stimulated Brillouin scattering," New J. Phys. **19**(1), 011003 (2017).
18. V. V. Spirin, C. A. López-Mercado, P. Mégret, and A. A. Fotiadi, "Single-mode Brillouin fiber laser passively stabilized at resonance frequency with self-injection locked pump laser," Laser Phys. Lett. **9**(5), 377–380 (2012).
19. B. J. Eggleton, C. G. Poulton, P. T. Rakich, M. J. Steel, and G. Bahl, "Brillouin integrated photonics," Nat. Photonics **13**(10), 664–677 (2019).
20. H. H. Diamandi and A. Zadok, "Ultra-narrowband integrated brillouin laser," Nat. Photonics **13**(1), 9–10 (2019).
21. S. Gundavarapu, G. M. Brodnik, M. Puckett, T. Huffman, D. Bose, R. Behunin, J. Wu, T. Qiu, C. Pinho, N. Chauhan, J. Nohava, P. T. Rakich, K. D. Nelson, M. Salit, and D. J. Blumenthal, "Sub-hertz fundamental linewidth photonic integrated brillouin laser," Nat. Photonics **13**(1), 60–67 (2019).
22. B. J. Eggleton, B. Luther-Davies, and K. Richardson, "Chalcogenide photonics," Nat. Photonics **5**(3), 141–148 (2011).
23. M. Merklein, B. Stiller, I. V. Kabakova, U. S. Mutugala, K. Vu, S. J. Madden, and R. Slavík, "Widely tunable, low phase noise microwave source based on a photonic chip," Opt. Lett. **41**(20), 4633–4636 (2016).
24. H. Shin, W. Qiu, R. Jarecki, J.A. Cox, R.H. Olsson III, A. Starbuck, and P.T. Rakich, "Tailorable stimulated Brillouin scattering in nanoscale silicon waveguides," Nat. Commun. **4**(1), 1944 (2013).
25. W. Loh, A. A. S. Green, F. N. Baynes, D. C. Cole, F. J. Quinlan, H. Lee, K. J. Vahala, S. B. Papp, and S. A. Diddams, "Dual-microcavity narrow-linewidth brillouin laser," Optica **2**(3), 225–232 (2015).
26. J. Li, X. Yi, H. Lee, S.A. Diddams, and K.J. Vahala, "Electro-optical frequency division and stable microwave synthesis," Science **345**(6194), 309–313 (2014).
27. M. R. Foreman, J. D. Swaim, and F. Vollmer, "Whispering gallery mode sensors," Adv. Opt. Photonics **7**(2), 168–240 (2015).
28. S. R. Mirnaziry, C. Wolff, M. Steel, B. Morrison, B. J. Eggleton, and C. G. Poulton, "Lasing in ring resonators by stimulated brillouin scattering in the presence of nonlinear loss," Opt. Express **25**(20), 23619–23633 (2017).
29. S. R. Mirnaziry, C. Wolff, M. J. Steel, B. J. Eggleton, and C. G. Poulton, "Stimulated brillouin scattering in integrated ring resonators," J. Opt. Soc. Am. B **34**(5), 937–949 (2017).
30. C. Wolff, P. Gutsche, M. J. Steel, B. J. Eggleton, and C. G. Poulton, "Power limits and a figure of merit for stimulated brillouin scattering in the presence of third and fifth order loss," Opt. Express **23**(20), 26628–26638 (2015).
31. N. T. Otterstrom, R. O. Behunin, E. A. Kittlaus, Z. Wang, and P. T. Rakich, "A silicon brillouin laser," Science **360**(6393), 1113–1116 (2018).
32. B. Morrison, A. Casas-Bedoya, G. Ren, K. Vu, Y. Liu, A. Zarifi, T. G. Nguyen, D.-Y. Choi, D. Marpaung, and S. J. Madden, "Compact brillouin devices through hybrid integration on silicon," Optica **4**(8), 847–854 (2017).
33. I. V. Kabakova, R. Pant, D.-Y. Choi, S. Debbarma, B. Luther-Davies, S. J. Madden, and B. J. Eggleton, "Narrow linewidth brillouin laser based on chalcogenide photonic chip," Opt. Lett. **38**(17), 3208–3211 (2013).
34. C. Wolff, B. Stiller, B. J. Eggleton, M. J. Steel, and C. G. Poulton, "Cascaded forward brillouin scattering to all stokes orders," New J. Phys. **19**(2), 023021 (2017).
35. J. Li, M.-G. Suh, and K. Vahala, "Microresonator brillouin gyroscope," Optica **4**(3), 346–348 (2017).
36. W. Loh, S. B. Papp, and S. A. Diddams, "Noise and dynamics of stimulated-Brillouin-scattering microresonator lasers," Phys. Rev. A **91**(5), 053843 (2015).
37. H. A. Haus, *Waves and Fields in Optoelectronics* (Prentice-Hall, 1983).
38. J. Li, H. Lee, T. Chen, and K. J. Vahala, "Characterization of a high coherence, Brillouin microcavity laser on silicon," Opt. Express **20**(18), 20170–20180 (2012).
39. R. W. Boyd, K. Rzaewski, and P. Narum, "Noise initiation of stimulated Brillouin scattering," Phys. Rev. A **42**(9), 5514–5521 (1990).
40. C. E. Preda, A. A. Fotiadi, and P. Mégret, "Numerical approximation for brillouin fiber ring resonator," Opt. Express **20**(5), 5783 (2012).